# A sixth-order dual preserving algorithm for the Camassa-Holm equation

Pao-Hsiung Chiu* Long Lee† Tony W. H. Sheu‡

November 6, 2009

**Abstract**

The paper presents a sixth-order numerical algorithm for studying the completely integrable Camass-Holm (CH) equation. The proposed sixth-order accurate method preserves both the dispersion relation and the Hamiltonians of the CH equation. The CH equation in this study is written as an evolution equation, involving only the first-order spatial derivatives, coupled with the Helmholtz equation. We propose a two-step method that first solves the evolution equation by a sixth-order symplectic Runge-Kutta method and then solves the Helmholtz equation using a three-point sixth-order compact scheme. The first-order derivative terms in the first step are approximated by a sixth-order dispersion-relation-preserving scheme that preserves the physically inherent dispersive nature. The compact Helmholtz solver, on the other hand, allows us to use relatively few nodal points in a stencil, while achieving a higher-order accuracy. The sixth-order symplectic Runge-Kutta time integrator is preferable for an equation that possess a Hamiltonian structure. We illustrate the ability of the proposed scheme by examining examples involving peakon or peakon-like solutions. We compare the computed solutions with exact solutions or asymptotic predictions. We also demonstrate the ability of the symplectic time integrator to preserve the Hamiltonians. Finally, via a smooth travelling wave problem, we compare the accuracy, elapsed computing time, and rate of convergence among the proposed method, a second-order two-step algorithm, and a completely integrable particle method.

**keywords:** Camassa-Holm equation; Hamiltonians; symplectic Runge Kutta; sixth-order; Helmholtz equation; dispersion-relation-preserving.

## 1 Introduction

The Camassa-Holm (CH) equation [2],

$$u_t + 2\kappa u_x - u_{xxt} + 3uu_x = 2u_x u_{xx} + uu_{xxx}, \tag{1.1}$$

results from an asymptotic expansion of the Euler equations governing the motion of an inviscid fluid whose free surface can exhibit gravity-driven wave motion [3, 17]. The small parameters used to carry out the

*Department of Engineering Science and Ocean Engineering, National Taiwan University, No. 1, Sec. 4, Roosevelt Rd., Da-an District, Taipei City 106, Taiwan (R.O.C.). E-mail : f93525011@ntu.edu.tw

†Department of Mathematics, Ross Hall 212, University of Wyoming, Dept 3036, 1000 E. University Ave., Laramie, WY 82071-3036, USA. E-mail : llee@uwyo.edu

‡Department of Engineering Science and Ocean Engineering, National Taiwan University, No. 1, Sec. 4, Roosevelt Rd., Da-an District, Taipei City 106, Taiwan (R.O.C.). E-mail : twhsheu@ntu.edu.tw

expansion are the aspect ratio, whereby the depth of the fluid is assumed to be much smaller than the typical wavelength of the motion, and the amplitude ratio, or ratio between a typical amplitude of wave motion and the average depth of the fluid. Thus, the equation is a member of the class of weakly nonlinear (due to the smallness assumption on the amplitude parameter) and weakly dispersive (due to the long wave assumption parameter) models for water wave propagation. However, at variance with its celebrated close relatives in this class, such as the Korteweg-de Vries (KdV) and Benjamin-Bona-Mahony (BBM) equations, these small parameters are assumed to be linked only by a relative ordering, rather than by a power-law relation. This allows us to retain terms on the right-hand-side that would be of higher order with respect to both the KdV and BBM expansions, and, in principle, to consider dynamical regimes in which nonlinearity is somewhat dominant with respect to wave dispersion. This equation possesses the remarkable property of complete integrability, as evidenced by its Lax-pair representation, and permits an infinite number of nonlocal conserved properties [2, 20]. When $\kappa = 0$ in equation (1.1), the equation becomes a non-dispersive equation that admits peakon solutions.

There is extensive literature on numerical analysis and implementation for the KdV type of equations; however, numerical algorithms for the CH equation have only received attention recently. While no attempt will be made here to provide a detailed reference list, the following are examples of recent algorithms developed for the CH equation. In [5–9], a completely integrable particle method is introduced that solves the equation in infinite domains, semi-infinite domains with the zero boundary condition on one side, periodic domains, and homogeneous finite domains. The particle method is based on the Hamiltonian structure of the equation, an algorithm corresponding to a completely integrable particle lattice. Each particle in this method travels along a characteristic curve of the shallow-water wave model, determined by solving a system of nonlinear integro-differential equations. This system of nonlinear integro-differential equations can be viewed as particle interaction through a long-range potential (here position and momentum dependent). Besides the particle method, a method based on multipeakons is developed in [15] for equation (1.1). The convergence proof of this method is given in [16]. A pseudospectral method is developed in [18] for the travelling wave solution of equation (1.1). Similar methods, a semi-discretization Fourier-Galerkin method and a Fourier-collocation method, are developed in [19]. A finite volume method, within the adaptive upwinding context, is developed for the peakon solution of equation (1.1) [1]. A local discontinuous Galerkin finite element method is developed in [23].

Equation (1.1) involves two third-order derivative terms, $uu_{xxx}$ and $u_{xxt}$. For most numerical schemes, except the particle method and the related methods, certain care is required to discretize those terms in order to achieve a higher-order accuracy while preserving the physically inherent dispersive nature of the equation. In the study, however, we avoid discretizing both of the third-order derivative terms by applying the Helmholtz operator to $u$

$$m(x,t) \equiv (1-\partial_x^2)\, u(x,t), \tag{1.2}$$

and rewrite the equation (1.1) into an equivalent formulation

$$m_t = -2(m+\kappa)\, u_x - u m_x. \tag{1.3}$$

We call equations (1.2) and (1.3) the $m$-formulation of the CH equation. Note that equation (1.3) involves only the first-order derivative terms. As a result of the new formulation, we develop a sixth-order two-step iterative numerical algorithm that first solves the evolution equation (1.3) by a sixth-order symplectic Runge-Kutta method and then solves the Helmholtz equation (1.2) with a three-point sixth-order compact scheme. The first-order derivative terms in the first step are approximated by a sixth-order dispersion-relation-preserving scheme that preserves the physically inherent dispersive nature. The compact Helmholtz

solver, on the other hand, allows us to use relatively few nodal points in a stencil, while achieving a higher-order accuracy. The sixth-order symplectic Runge-Kutta time integrator preserves the Hamiltonians of the equation. The principle of the two-step iterative algorithm is to solve the first-order equation and then to solve the Helmholtz equation, repeating the process until the convergence criterions are satisfied. A second-order accurate scheme based on the same principle for solving the CH equation and a class of partial differential equations involving the Helmholtz equation is developed in [10, 11].

## 2 Two-step iterative algorithm

The evolution equation (1.3) can be solved by a standard method of lines (MOL). Let $m^n = m(t^n, x)$ and $m^{n+1} = m(t^n + \Delta t, x)$ be the semi-discretized $m$ values at time level $n$ and $n+1$, respectively. Letting $F(m,u) = (-2\kappa u_x - u m_x - 2u_x m)$, equation (1.3) becomes

$$m_t = F(m,u). \tag{2.1}$$

A sixth-order accurate symplectic Runge-Kutta scheme, developed in [21], is employed in the MOL for solving equation (2.1):

$$m^{(1)} = m^n + \Delta t \left[ \frac{5}{36} F^{(1)} + (\frac{2}{9} + \frac{2\tilde{c}}{3}) F^{(2)} + (\frac{5}{36} + \frac{\tilde{c}}{3}) F^{(3)} \right], \tag{2.2}$$

$$m^{(2)} = m^n + \Delta t \left[ (\frac{5}{36} - \frac{5\tilde{c}}{12}) F^{(1)} + (\frac{2}{9}) F^{(2)} + (\frac{5}{36} + \frac{5\tilde{c}}{12}) F^{(3)} \right], \tag{2.3}$$

$$m^{(3)} = m^n + \Delta t \left[ (\frac{5}{36} - \frac{\tilde{c}}{3}) F^{(1)} + (\frac{2}{9} - \frac{2\tilde{c}}{3}) F^{(2)} + \frac{5}{36} F^{(3)} \right], \tag{2.4}$$

$$m^{n+1} = m^n + \Delta t \left[ \frac{5}{18} F^{(1)} + \frac{4}{9} F^{(2)} + \frac{5}{18} F^{(3)} \right]. \tag{2.5}$$

where $\tilde{c} = \frac{1}{2}\sqrt{\frac{3}{5}}$ and $F^{(i)} = F(m^{(i)}, u^{(i)})$, $i = 1,2,3$. In this symplectic Runge-Kutta method, in order to obtain $m^{n+1}$ from equation (2.5), we need to solve equations (2.2) $-$ (2.4) simultaneously for obtaining $m^{(1)}$, $m^{(2)}$, and $m^{(3)}$. After obtaining $m^{n+1}$, we solve the Helmholtz equation to obtain $u^{n+1}$. However, since the evolution equation (2.1) is coupled with the Helmholtz equation (1.2), in order to obtain $m^{n+1}$ and $u^{n+1}$ from $m^n$ and $u^n$, it is necessary to introduce an iterative scheme. Therefore, instead of forming a linear system and solving equations (2.2) $-$ (2.4) simultaneously, we incorporate the three equations into an iterative scheme. The iterative scheme solves equation (2.1) and the Helmholtz equation alternately until the convergence criterions are satisfied. The iterative steps are described as follows:

- **Step 1**: $m^n$ and $u^n$ are known. We perform the fixed-point iteration on equations (2.2) $-$ (2.4) to obtain $m^{(i)}$:

  (I) Given an initial guess for $m^{(i)}$ and $u^{(i)}$, denoted $m^{[0],(i)}$ and $u^{[0],(i)}$, respectively, $i = 1,2,3$ from $m^n$ and $u^n$. Solve equations (2.2) $-$ (2.4) to obtain $m^{[1],(i)}$, $i = 1,2,3$.

  (II) Using $m^{[1],(i)}$ and the three-point sixth-order compact scheme, we solve the Helmholtz equation (1.2) to obtain $u^{[1],(i)}$, $i = 1,2,3$.

(III) Repeat (I) with $u^{[k],(i)}$ and $m^{[k],(i)}$ and (II) for the next iteration until the $(k+1)^{th}$ iteration, for which the residuals, in the maximum norm, of equations (2.2) − (2.4) and the Helmholtz equation (1.2) satisfy our convergence criterions:

$$\begin{aligned} \max_{x_{j,j=1,N}} \left| \frac{m^{[k+1],(i)} - m^n}{\Delta t} - F\left(m^{[k+1],(i)}, u^{[k+1],(i)}\right) \right| \leq \varepsilon, \\ \max_{x_{j,j=1,N}} \left| m^{[k+1],(i)} - \left(u^{[k+1],(i)} - u_{xx}^{[k+1],(i)}\right) \right| \leq \varepsilon, \end{aligned} \tag{2.6}$$

where $N$ is the number of grid points and $i = 1,2,3$. The value for the threshold error $\varepsilon$ is typically chosen to be $10^{-12}$ throughout our computations. Our numerical experiments indicate that typically the number of iterations needed for convergence is less than 20 (i.e. $k+1 \leq 20$).

- **Step 2**: Use equation (2.5) to update $m^{n+1}$.
- **Step 3**: Solve equation (1.2) to obtain $u^{n+1}$. Return to **Step 1**.

# 3 Dispersion-relation-preserving scheme

The spacial accuracy of the proposed scheme depends on how accurately we can approximate the first-order derivative terms. In particular, if the equation of interest is a dispersive equation, such as the CH equation, a dispersion-relation-preserving scheme is necessary to ensure the accuracy of numerical solutions. In this section, we develop a dispersion-relation-preserving scheme for the first-order derivative terms.

Suppose that the first derivative term at the grid point $i$ is approximated by the following algebraic equation:

$$\begin{aligned} \frac{\partial m}{\partial x}|_i = \frac{1}{h}(c_1 m_{i-5} + c_2 m_{i-4} + c_3 m_{i-3} + c_4 m_{i-2} + c_5 m_{i-1} \\ + c_6 m_i + c_7 m_{i+1} + c_8 m_{i+2} + c_9 m_{i+3}). \end{aligned} \tag{3.1}$$

For simplicity, we consider the case involving only the positive convective coefficient in the above equation, since the derivation will be the same for the negative convective coefficient.

Derivation of expressions for $c_1 \sim c_9$ is followed by applying the Taylor series expansions for $m_{i\pm1}$, $m_{i\pm2}$, $m_{i\pm3}$, $m_{i-4}$ and $m_{i-5}$ with respect to $m_i$ and then eliminating the seven leading error terms derived in the modified equation. Elimination of these error terms enables us to derive the following set of algebraic equations:

$$c_1 + c_2 + c_3 + c_4 + c_5 + c_6 + c_7 + c_8 + c_9 = 0, \tag{3.2}$$

$$-5c_1 - 4c_2 - 3c_3 - 2c_4 - c_5 + c_7 + 2c_8 + 3c_9 = 1, \tag{3.3}$$

$$\frac{25}{2}c_1 + 8c_2 + \frac{9}{2}c_3 + 2c_4 + + \frac{1}{2}c_5 \frac{1}{2}c_7 + 2c_8 + \frac{9}{2}c_9 = 0, \tag{3.4}$$

$$-\frac{125}{6}c_1 - \frac{32}{3}c_2 - \frac{9}{2}c_3 - \frac{4}{3}c_4 - \frac{1}{6}c_5 + \frac{1}{6}c_7 + \frac{4}{3}c_8 + \frac{9}{2}c_9 = 0, \tag{3.5}$$

$$\frac{625}{24}c_1 + \frac{32}{3}c_2 + \frac{27}{8}c_3 + \frac{2}{3}c_4 + \frac{1}{24}c_5 + \frac{1}{24}c_7 + \frac{2}{3}c_8 + \frac{27}{8}c_9 = 0, \tag{3.6}$$

$$-\frac{625}{24}c_1 - \frac{128}{15}c_2 - \frac{81}{40}c_3 - \frac{4}{15}c_4 - \frac{1}{120}c_5 + \frac{1}{120}c_7 + \frac{4}{15}c_8 + \frac{81}{40}c_9 = 0, \tag{3.7}$$

$$\frac{3125}{144}c_1 + \frac{256}{45}c_2 + \frac{81}{80}c_3 + \frac{4}{45}c_4 + \frac{1}{720}c_5 + \frac{1}{720}c_7 + \frac{4}{45}c_8 + \frac{81}{80}c_9 = 0. \tag{3.8}$$

To uniquely determine all nine introduced coefficients shown in (3.1), we need two more equations. Following the suggestion in [22], we derive the equations by preserving the dispersion relation that governs the relation between the angular frequency and the wavenumber of the first-order dispersive term. To obtain the two extra equations based on the principle of preservation of the dispersion relation, we note that the Fourier transform pair for $m$ is

$$\tilde{m}(k) = \frac{1}{2\pi} \int_{-\infty}^{+\infty} m(x)\, e^{-\mathbf{i}kx}\, dx, \tag{3.9}$$

$$m(x) = \int_{-\infty}^{+\infty} \tilde{m}(\alpha)\, e^{\mathbf{i}kx}\, dk. \tag{3.10}$$

If we perform the Fourier transform on each term shown in Eq. (3.1), we obtain that the wavenumber $k$ is approximated by the following expression

$$\begin{aligned} k \simeq \frac{-\mathbf{i}}{h}(&c_1\, e^{-\mathbf{i}5kh} + c_2\, e^{-\mathbf{i}4kh} + c_3\, e^{-\mathbf{i}3kh} + c_4\, e^{-\mathbf{i}2kh} + c_5\, e^{-\mathbf{i}kh} \\ &+ c_6 + c_7\, e^{\mathbf{i}kh} + c_8\, e^{\mathbf{i}2kh} + c_9\, e^{\mathbf{i}3kh}), \end{aligned} \tag{3.11}$$

where $\mathbf{i} = \sqrt{-1}$.

Supposing that the effective wavenumber $\tilde{k}$ is exactly equal to the right-hand side of Eq. (3.11) [22], we have $k \approx \tilde{k}$. In order to acquire a better dispersive accuracy, $\tilde{k}$ should be made as close to $k$ as possible. This implies that $E$ defined in the sense of the 2-norm of the error between $k$ and $\tilde{k}$ will be the local minimum for such a $\tilde{k}$. The error $E$ is defined as follows

$$E(k) = \int_{-\frac{\pi}{2}}^{\frac{\pi}{2}} \left|\, kh - \tilde{k}h \,\right|^2\, d(kh) = \int_{-\frac{\pi}{2}}^{\frac{\pi}{2}} |\, \gamma - \tilde{\gamma} \,|^2\, d\gamma, \tag{3.12}$$

where $h$ is denoted as the grid size and $\gamma = kh$. For $E$ to be a local minimum, we assume the following two extreme conditions

$$\frac{\partial E}{\partial c_4} = 0, \tag{3.13}$$

$$\frac{\partial E}{\partial c_5} = 0. \tag{3.14}$$

Under the above prescribed extreme conditions, the two algebraic equations needed for the coefficients to be uniquely determined are

$$-\frac{4}{3}c_1 + 4c_3 + 2\pi c_4 + 4c_5 - \frac{4}{3}c_7 + \frac{4}{5}c_9 + \pi = 0, \tag{3.15}$$

$$-\frac{4}{3}c_2 + 4c_4 + 2\pi c_5 + 4c_6 - \frac{4}{3}c_8 + 4 = 0. \tag{3.16}$$

We remark that for a truly dispersion-relation-preserving scheme, *i.e.* the error $E$ is truly a local minimum on the parameter space, one will need to impose $\partial E/\partial c_i = 0$ for $i = 1...9$ to obtain 9 equations for the coefficients. Our approach, instead, (i) ensures the higher-order accuracy by letting the coefficients satisfy the Taylor series expansions and (ii) partially enforces the requirements for a dispersion-relation-preserving scheme. Our numerical experiments show that the upwinding scheme for the first-order derivative obtained by taking the derivatives about $c_4$ and $c_5$ for $E$ (equations (3.13) and (3.14)) produces the least numerical

errors. It is also worth noting that the integration interval shown in equation (3.12) needs to be sufficiently wide to cover a complete period of sine (or cosine) waves.

Equations (3.15) and (3.16) together with equations (3.2) to (3.8) yield the coefficients :

$$c_1 = \frac{1}{50}\left(\frac{1575\pi^2 - 8340\pi + 10624}{-12432\pi + 17408 + 2205\pi^2}\right), \tag{3.17}$$

$$c_2 = -\frac{3}{100}\left(\frac{7875\pi^2 - 42480\pi + 55552}{-12432\pi + 17408 + 2205\pi^2}\right), \tag{3.18}$$

$$c_3 = \frac{1}{75}\left(\frac{55125\pi^2 - 303240\pi + 406976}{-12432\pi + 17408 + 2205\pi^2}\right), \tag{3.19}$$

$$c_4 = -\frac{1}{10}\left(\frac{-62160\pi + 85888 + 11025\pi^2}{-12432\pi + 17408 + 2205\pi^2}\right), \tag{3.20}$$

$$c_5 = -\frac{12}{5(21\pi - 64)}, \tag{3.21}$$

$$c_6 = -\frac{7}{100}\left(\frac{17325\pi^2 - 103440\pi + 153344}{-12432\pi + 17408 + 2205\pi^2}\right), \tag{3.22}$$

$$c_7 = \frac{1}{25}\left(\frac{55125\pi^2 - 318360\pi + 457664}{-12432\pi + 17408 + 2205\pi^2}\right), \tag{3.23}$$

$$c_8 = -\frac{9}{50}\left(\frac{2625\pi^2 - 15440\pi + 22656}{-12432\pi + 17408 + 2205\pi^2}\right), \tag{3.24}$$

$$c_9 = \frac{1}{6}\left(\frac{15\pi - 44}{105\pi - 272}\right). \tag{3.25}$$

It is easy to show that the proposed upwinding scheme for the first-order derivative is sixth-order spatially accurate :

$$\begin{aligned}\frac{\partial m}{\partial x} = \frac{\partial m}{\partial x}|_{exact} &- \frac{48}{175}\left(\frac{105\pi - 332}{-12432\pi + 17408 + 2205\pi^2}\right)h^6 \frac{\partial^7 m}{\partial x^7} \\ &+ \left(\frac{7875\pi^2 - 39360\pi + 45824}{-12432\pi + 17408 + 2205\pi^2}\right)h^7 \frac{\partial^8 m}{\partial x^8} + O(h^8) + \cdots .\end{aligned} \tag{3.26}$$

# 4 Three-point sixth-order accurate compact Helmholtz solver

We introduce a compact scheme for solving the Helmholtz equation in this section. It is well known that in order to obtain a higher-order numerical method for the Helmholtz equation, one can always introduce more points in a stencil. The improved accuracy, however, comes at the cost of an expensive matrix calculation, due to the wider stencil. With the aim of developing a numerical scheme that is higher-order accurate while using relative few stencil points in the finite difference discretization, we introduce a compact scheme involving only three points in a stencil, but is sixth-order accurate.

Consider the following prototype equation

$$\frac{\partial^2 u}{\partial x^2} - ku = f(x). \tag{4.1}$$

We first denote the values of $\partial^2 u/\partial x^2$, $\partial^4 u/\partial x^4$ and $\partial^6 u/\partial x^6$ at a nodal point $i$ as

$$\frac{\partial^2 u}{\partial x^2}|_i = s_i, \tag{4.2}$$

$$\frac{\partial^4 u}{\partial x^4}|_i = v_i, \tag{4.3}$$

$$\frac{\partial^6 u}{\partial x^6}|_i = w_i. \tag{4.4}$$

Development of the compact scheme at point $i$ starts with relating $v$, $s$ and $w$ with $u$ as follows:

$$\delta_0 h^6 w_i + \gamma_0 h^4 v_i + \beta_0 h^2 s_i = \alpha_1 u_{i+1} + \alpha_0 u_i + \alpha_{-1} u_{i-1}. \tag{4.5}$$

Based on physics, it is legitimate to set $\alpha_1 = \alpha_{-1}$ since the Helmholtz equation is elliptic in nature. Having set $\alpha_1 = \alpha_{-1}$, the derivation is followed by expanding $u_{i\pm1}$ with respect to $u_i$. Substitution of these Taylor-series expansion equations into Eq. (4.5) leads to

$$\begin{aligned}
&\delta_0 h^6 w_i + \gamma_0 h^4 v_i + \beta_0 h^2 s_i \\
&= (\alpha_0 + 2\alpha_1) u_i + \frac{h^2}{2!}(2\alpha_1)\frac{\partial^2 u_i}{\partial x^2} + \frac{h^4}{4!}(2\alpha_1)\frac{\partial^4 u_i}{\partial x^4} + \frac{h^6}{6!}(2\alpha_1)\frac{\partial^6 u_i}{\partial x^6} + \frac{h^8}{8!}(2\alpha_1)\frac{\partial^8 u_i}{\partial x^8} + \cdots .
\end{aligned} \tag{4.6}$$

Through a term-by-term comparison of the derivatives shown in Eq. (4.6), five simultaneous algebraic equations can be derived. Hence, the introduced free parameters can be determined as $\alpha_1 = \alpha_{-1} = -1$, $\alpha_0 = 2$, $\beta_0 = -1$, $\gamma_0 = -\frac{1}{12}$ and $\delta_0 = -\frac{1}{360}$. Note that $w_i = k^3 u_i + k^2 f_i + k\frac{\partial^2 f_i}{\partial x^2} + \frac{\partial^4 f_i}{\partial x^4}$, $v_i = k^2 u_i + k f_i + \frac{\partial^2 f_i}{\partial x^2}$, and $s_i = k\,u_i + f_i$. Equation (4.5) can then be expressed as

$$\begin{aligned}
&\alpha_1 u_{i+1} + \left(\alpha_0 - \beta_0 h^2 k - \gamma_0 h^4 k^2 - \delta_0 h^6 k^3\right) u_i + \alpha_1 u_{i-1} \\
&= \left[ h^2 \beta_0 f_i + h^4 \gamma_0 \left( k f_i + \frac{\partial^2 f_i}{\partial x^2} \right) + h^6 \delta_0 \left( k^2 f_i + k\frac{\partial^2 f_i}{\partial x^2} + \frac{\partial^4 f_i}{\partial x^4} \right) \right].
\end{aligned} \tag{4.7}$$

It follows that

$$\begin{aligned}
&u_{i+1} - \left(2 + h^2 k + \frac{1}{12} h^4 k^2 + \frac{1}{360} h^6 k^3\right) u_i + u_{i-1} \\
&= h^2 f_i + \frac{1}{12} h^4 \left( k f_i + \frac{\partial^2 f_i}{\partial x^2} \right) + \frac{1}{360} h^6 \left( k^2 f_i + k\frac{\partial^2 f_i}{\partial x^2} + \frac{\partial^4 f_i}{\partial x^4} \right).
\end{aligned} \tag{4.8}$$

Using the proposed scheme, the corresponding modified equation for (4.1) can be derived as follows, after performing some algebraic manipulation:

$$\frac{\partial^2 u}{\partial x^2} - k\,u = f + \frac{h^6}{20160}\frac{\partial^8 u}{\partial x^8} + \frac{h^8}{1814400}\frac{\partial^{10} u}{\partial x^{10}} + \cdots + H.O.T.. \tag{4.9}$$

Equation (4.9) shows that the 3-point stencil scheme is indeed sixth-order accurate. We implement a multi-grid method using the V-cycle and fully-weighted projection/prolongation with the red-black Gauss-Seidel smoother to solve the system of algebraic equations arising from discretization of the proposed scheme.

# 5 Numerical results

In this section, we provide several test problems to validate the proposed scheme and elucidate its computational properties.

### 5.1 Travelling wave solution in periodic domains

The first example is the traveling wave solution in periodic domains considered in [8, 9]. The periodic travelling wave solution is given by $u(x,t) = U(x - ct)$, provided that the minima of $u$ are located at $u = 0$ and the wave elevation is positive. In this case one finds the solution of the travelling wave equation is given by

$$U' = \pm \sqrt{\frac{-U^3 + (c - 2\kappa)U^2 + C(A)\,U}{c - U}}, \tag{5.1}$$

where $c$ and $A$ are denoted as the wave speed and the wave amplitude, respectively, and the integration constant $C$ is a function of $A$. Integration of equation (5.1) leads to the expression,

$$x = \frac{2}{\sqrt{b_1(b_2 - b_3)}}(b_1 - b_2)\Pi(\varphi, \beta^2, T). \tag{5.2}$$

The wavelength $L$ of this periodic solution can be written as

$$L = \frac{4}{\sqrt{b_1(b_2 - b_3)}}(b_1 - b_2)\Pi(\varphi, \beta^2, T). \tag{5.3}$$

Details about the variable $x$, $\varphi$, $\beta$, $b_i\,(i = 1 \cdots 3)$, $c$, and $T$ are discussed in [8, 9].

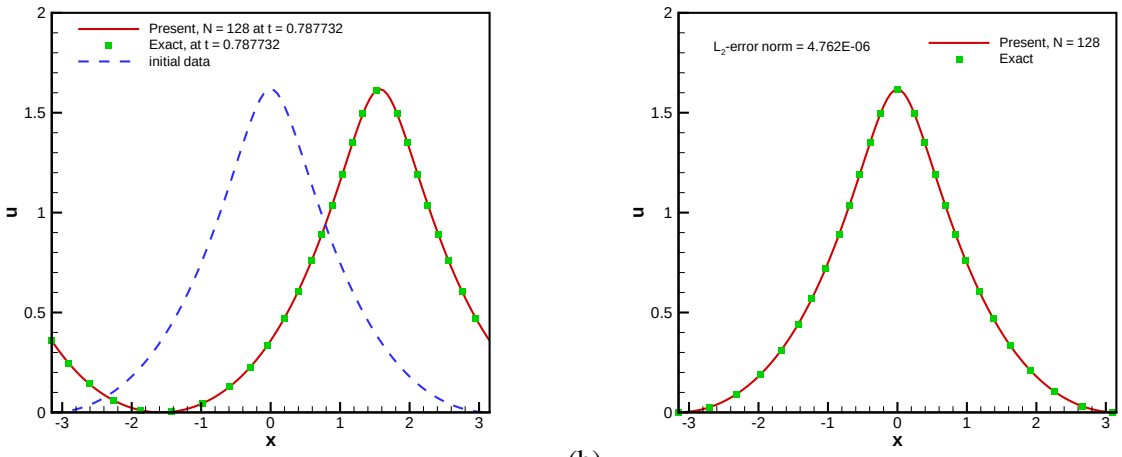


(a) (b)

Figure 5.1: The predicted traveling wave solution at (a) $t = 0.787732$, (b) $t = 3.1509$ (over one period). Both are compared with the exact solution, the dotted lines. The domain is $L \approx 6.3019$. The number of cells used for this calculation is $N = 128$ and $\Delta t = \frac{1}{4}\Delta x$.

The parameters used in the test problem are $c = 2$, $\kappa = 1/2$, and the integration constant $C = 1$, which altogether yield the wavelength (period) of $L \approx 6.3019$ according to equation (5.3). The total time for the wave to travel through the domain and back to the initial position is $t = 3.1509$. The time step used in this calculation is $\Delta t = \frac{1}{4}\Delta x$ while the grid size is $\Delta x = 0.0492$ (or the number of cells $N = 128$). Figure 5.1(a) shows the numerical and the exact solutions at $t = 0.788$. The initial data is the dashed line. A good

| | error in $L_2$ norm | | |
|---|---|---|---|
| number of cells | current method | $2^{nd}$-order two-step iterative method | particle method |
| $N = 32$ | 4.36E-03 | 6.83E-03 | 1.34E-02 |
| $N = 64$ | 2.02E-04 | 9.08E-04 | 3.19E-03 |
| $N = 128$ | 4.76E-06 | 2.56E-04 | 7.53E-04 |
| $N = 256$ | 5.70E-08 | 6.47E-05 | 1.90E-04 |

Table 5.1: The comparison of errors in $L_2$ norm among three methods for the problem considered in Figure 5.1 (b). The time step used in the calculation is $c\frac{\Delta t}{\Delta x} = \frac{1}{4}$.

| | rate of convergence | | |
|---|---|---|---|
| number of cells | current method | $2^{nd}$-order two-step iterative method | particle method |
| $N = 32$ | — | — | — |
| $N = 64$ | 4.43 | 2.91 | 2.07 |
| $N = 128$ | 5.41 | 1.82 | 2.08 |
| $N = 256$ | 6.38 | 1.98 | 1.98 |

Table 5.2: The comparison of rates of convergence among three methods for the problem considered in Figure 5.1 (b). The time step used in the calculation is $c\frac{\Delta t}{\Delta x} = \frac{1}{4}$.

| | CPU times (seconds) | | |
|---|---|---|---|
| number of cells | current method | $2^{nd}$-order two-step iterative method | particle method |
| $N = 32$ | 9.37E-02 | 4.69E-02 | $\leq$ 1.0E-03 |
| $N = 64$ | 3.59E-01 | 1.56E-01 | 1.56E-02 |
| $N = 128$ | 1.72 | 4.53E-01 | 3.12E-02 |
| $N = 256$ | 3.66 | 1.16 | 1.41E-01 |

Table 5.3: The comparison of CPU times among three methods for the problem considered in Figure 5.1 (b). The time step used in the calculation is $c\frac{\Delta t}{\Delta x} = \frac{1}{4}$.

agreement with the analytic solution is clearly demonstrated. To show that the proposed scheme is phase accurate, we also plot the predicted solution at $t = 3.1509$. As Figure 5.1(b) is shown, the waveform over one period of time and the waveform of the initial data are visually identical. Tables 5.1 − Table 5.3 show the comparisons of errors in $L_2$ norm, rates of convergence, and CPU times among three different methods: the proposed method, a second-order two-step iterative method [11], and a second-order particle method [9]. The solutions are computed at a fixed ratio $c\frac{\Delta t}{\Delta x} = 0.25$, where $c = 2$ is the wave speed. As expected, the tables show that the proposed method is sixth-order accurate and has smallest errors in $L_2$ norm among the three methods for fine grids, but the proposed method is less efficient than the other two methods.

## 5.2 Smooth travelling wave solution

In [4], an exact travelling wave solution of equation (1.1) is given by $u(x,t) = U(x-ct) \equiv U(s)$, where $c = 8\kappa/3$ and

$$U(s) = \frac{8}{3}\kappa\left(1 - \frac{3\sqrt{3} + 6\sin 2z}{(1+2\cos 2z)(2\sqrt{3}\cos 2z - \sqrt{3}\cos 4z + 2\sin 2z + \sin 4z)}\right), \tag{5.4}$$

with $z = \arctan(e^{s/2})/3$. The initial condition $u_0(x) = U(x)$ yields the initial data for the auxiliary variable $m$,

$$m_0(x) = \kappa\left(\frac{c^2}{(c-U(x))^2} - 1\right). \tag{5.5}$$

The CH equation (1.1) is a complete integrable equation. There are many Hamiltonians associated with the equation. Among these conserved quantities, the mass $M$, and the Hamiltonians $H_1$ and $H_2$ are given as follows:

$$M = \int_{-\infty}^{\infty} u\,dx, \quad H_1 = \frac{1}{2}\int_{-\infty}^{\infty}\left(u^2 + (u_x)^2\right)\,dx, \quad H_2 = \frac{1}{2}\int_{-\infty}^{\infty}(u^3 + u(u_x)^2 + 2\kappa u^2)\,dx. \tag{5.6}$$

The conserved quantity $W$ associated with equation (1.1) is derived in [5]. The brief derivation for $W$ is described as follows. First, equation (1.1) is written as

$$\frac{\partial W_x}{\partial t} + \frac{\partial (uW_x)}{\partial x} = 0, \tag{5.7}$$

where $W_x$ is defined as $W_x = \sqrt{m+\kappa}$, where $m = u - u_{xx}$. If we define

$$W = \int_{-\infty}^{\infty} W_x\,dx, \tag{5.8}$$

then we can write equation (5.7) as

$$W_t + uW_x = 0. \tag{5.9}$$

This is an advection equation, where the conserved quantity $W$ is advected by $u$ and therefore is a constant in time. Figure 5.2 (a) is a plot for the computed travelling wave solution. The computed solution is compared with the exact solution at time $t = 50$ with $\kappa = 1$. The figure shows clearly that the computed solution and the exact solution are visually identical, which means that the proposed scheme evolves the solitary wave while perfectly maintaining its shape. Besides maintaining the waveform, the sixth-order symplectic time integrator employed in the proposed scheme has the ability to preserve the Hamiltonians. Figure 5.2 (b) shows that all the conserved quantities, $M$, $H_1$, $H_2$, and $W$, are well preserved by the proposed algorithm. The computational domain for this example is $[-180, 180]$, while the number of cells used is $N = 2048$ ($\Delta x = 0.17578$). The time step used is $\Delta t = 0.05$.

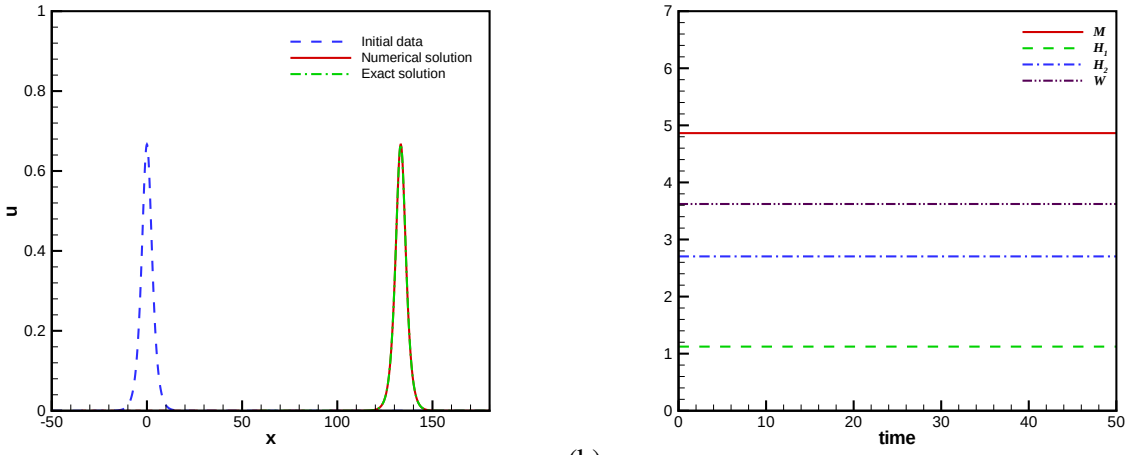


(a) (b)

Figure 5.2: (a) The smooth travelling wave. Comparison between the computed solution and the exact solution at $t = 50$. They are visually identical. (b) Verification of the proposed algorithm. It shows that the quantities $M$, $H_1$, $H_2$, and $W$ for the travelling wave problem in (a) are well preserved by the proposed algorithm. Note that the value of $W$ is divided by 100.

### 5.3 Interacting solitons

In [9], the CH equation (1.1) in periodic domains is scaled into the wave-dispersion regimes. Under this set of scales, equation (1.1) is compatible with the KdV equation studied in the paper by Zabusky and Kruskal [24]. Thus, the CH equation should in principle support solutions that behave similarly to those of the KdV equation and exhibit phenomena similar to those described in Zabusky and Kruskal's paper [24], i.e. soliton formation with interactions, and the recurrence of smooth initial states.

Consider the following scaled CH equation in a periodic domain:

$$\begin{aligned} &u_t + 2\kappa u_x - u_{xxt} + 3uu_x = 2u_x u_{xx} + uu_{xxx}, \\ &u(x,0) = \frac{1}{3\delta}\cos(\pi\delta x), \\ &u(0,t) = u(2/\delta, t), \end{aligned} \tag{5.10}$$

where $\kappa = 1/(2\delta)$ and $\delta^2$ is the small parameter in front of the dispersive term $u_{xxx}$ in the KdV equation. Note that when $\delta$ is small, the required periodic domain for the study is large. Hence a large number of grid points may be necessary for obtaining fully resolved computations, which makes the initial value problem (5.10) a challenging problem for a long-time behavior study. Using the parameter $\delta = 0.022$ in (5.10), Figure 5.3 (a) shows that eight solitons appear in the domain at the same time. The peaks and phases of the solitons are identical to those computed by the particle method. The number of cells used in this calculation is $N = 8192$ in the periodic domain $L = 2/\delta \approx 90.91$. The total number of time steps used is 3785 for the final time $t = 1.64$. Note that in order to use the result of the particle method as a referenced solution, we use a large number of particles, $N = 20001$, in our calculation. Similar to the example in the previous section, we also compute the conserved quantities, $M$, $H_1$, $H_2$, and $W$. We remark that in terms of preserving these conserved quantities, this example is a harder problem compared with the smooth travelling wave example in Section 5.2. The reason is that this example involves the formation of eight sharp solitons. Figure 5.3 (b)

shows that the proposed algorithm preserves all the conserved quantities during the formation of solitons. Note that in Figure 5.3 (b), the value of $H_1$ is divided by 1000, the value of $H_2$ is divided by 100000, and the value of $W$ is divided by 100.

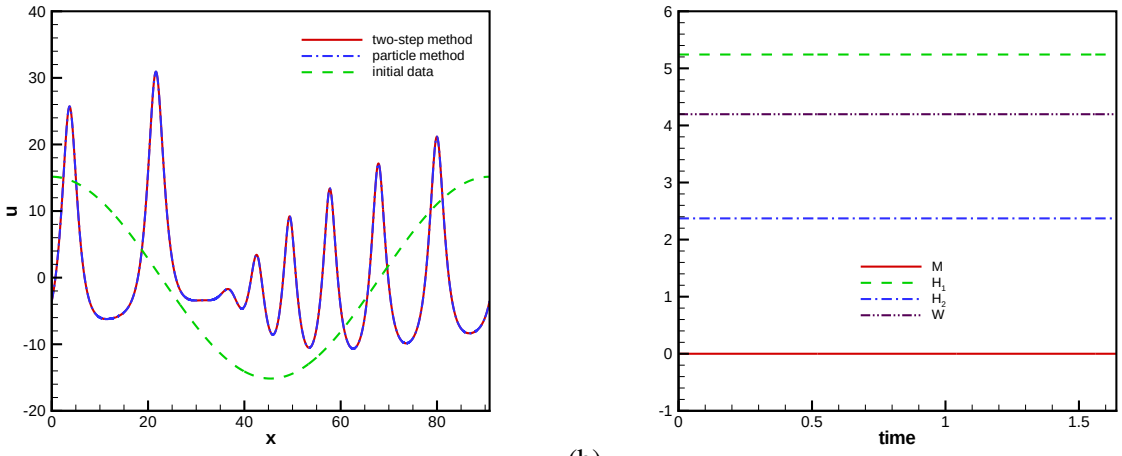


(a) (b)

Figure 5.3: (a) shows that eight solitons appear in the domain at the same time. The peaks and phases of the solitons are identical to those computed by the particle method. (b) shows that the proposed algorithm preserves all the conserved quantities during the formation of solitons.

## 5.4 The α-formulation

In the limit of $\kappa = 0$, the non-dispersive CH equation

$$u_t - u_{xxt} + 3uu_x = 2u_x u_{xx} + uu_{xxx} \tag{5.11}$$

admits peakon solutions. For peakon solutions, the second derivative of $u$ ($u_{xx}$) at the peaks is a Dirac delta function. Hence the auxiliary variable $m = u - u_{xx}$ is also a Dirac delta function. Therefore solving problems involving peakson solutions poses a challenge for the proposed $m$-formulation two-step algorithm. In fact, for problems of this type, numerical simulations pose a challenge as well to the Eulerian based schemes, including global spectral or pseudo-spectral schemes. A global spectral or pseudo-spectral scheme is definitely not a good choice for this type of problem, due to the huge number of terms required in the corresponding expansion (since the second derivative term of the sharp peaked wave is approaching to a Dirac delta function whose Fourier expansion coefficients do not decay).

In this study, to avoid this numerical difficulty, following the suggestion in [13], we write the non-dispersive CH equation (5.11) into an equivalent system of equations:

$$u_t + uu_x + P_x = 0, \tag{5.12}$$

$$-P_{xx} + P = \frac{1}{2}(u^2 + \alpha), \tag{5.13}$$

$$\alpha_t + (u\alpha)_x = (u^3 - 2Pu)_x, \tag{5.14}$$

where $\alpha = u^2 + u_x^2$. The two-step iterative method developed for solving equations (1.3) and (1.2), the $m$- formulation, can be used to solve the above system of equations. That is, in the first step, instead of

solving one equation (1.3), we solve equations (5.12) and (5.14) for $u$ and $\alpha$. In the second step, we solve a Helmholtz equation (5.13) for the auxiliary variable $P$. The dispersion-relation-preserving scheme, the three-point compact Helmholtz solver, and the symplectic sixth-order time integrator all remind unchanged. We call equations (5.12)-(5.14) the $\alpha$-formulation. Note that the $\alpha$-formulation involves estimating only the first-order spatial derivative of $u$. This is advantageous for problems involving peakon solutions, since the first-order spatial derivatives near the peaks can be accurately approximated by a finite difference approximation.

### 5.4.1 Sharp peaked travelling waves

An example in [5–7] shows that for the non-dispersive CH equation (5.11), the solution $u(x,t)$, corresponding to the initial condition $m_0(x) = a\,\mathrm{sech}^2(x)$, forms a rather sharply peaked wave and moves to the right, followed by others emerging from the location of the initial hump $m_0$. The peaks are sharpened over time and eventually the first-order spatial derivatives of the peaks become discontinuous (corners) when time approaches infinity. For the particle method developed in [5–7], one can observe that the particles rapidly cluster in the region of the peaks of the solitary waves. Such pile-up phenomenon suggests that particles get very close to each other in this region. When the distance between particles is so close that the machine precision can no longer distinguish between locations of the coalescing particles, *particle collisions* occur numerically. This effect is purely numerical, since particle collisions cannot take place in finite time [7]. As a consequence of such a numerical artifact, the particle method breaks down shortly after the numerical collision occurs. Nevertheless, because of the particle clustering, the particle method can capture the peak location accurately before the method breaks down. To resolve the numerical artifact, one can use a higher-precision arithmetic to extend the time for the first occurrence of such numerical particle collisions [7]. Besides higher-precision arithmetics, a redistribution algorithm is introduced in [7] to resolve the numerical particle collision, so that a lower-precision arithmetic can be used for solving the problem. We use results computed from the particle method as the referenced solutions.

We use $a = 1/2$ in the initial condition, $m_0(x) = a\,\mathrm{sech}^2(x)$, and solve the Helmholtz equation (1.2) to obtain $u_0$. Figure 5.4 (a) shows the first soliton, the second soliton, and the formation of the third soltion computed by the proposed algorithm with the $\alpha$-formulation. Figure 5.4 (b) is the magnification of the third soliton. The solutions computed by the proposed method is compared with those computed by the particle method. The results are indistinguishable between the two methods. The final time of the calculation is $t = 400$. The number of cells used for the proposed method is $N = 65536$ in the domain $[-50, 150]$ ($\Delta x \cong 0.00305176$), while the resolution for the particle method is $\Delta x = 0.0075$. The time step used is $\Delta t = 0.00125$ for the proposed method and $\Delta t = 0.00325$ for the particle method. Table 5.4 compares the magnitudes of the first and the second solitons computed by the proposed and the particle methods at $t = 400$, with those predicted by the theory as $t \to \infty$ [5]. Both methods have done a good job of predicting the magnitudes.

| | The proposed method (t=400) | The particle method (t=400) | Theoretical prediction ($t \to \infty$) |
|---|---|---|---|
| The first soliton | 0.332657 | 0.332359 | $1/3$ |
| The second soliton | 0.067200 | 0.066665 | $2/30$ |

Table 5.4: Comparison of the predicted magnitudes of the first and the second solitons among the proposed method, the particle method, and the theory.

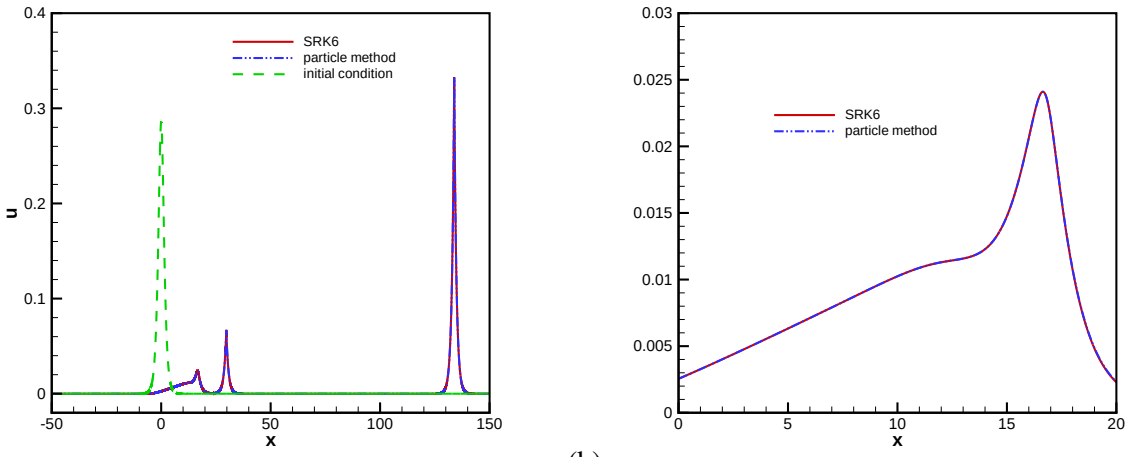


(a) (b)

Figure 5.4: (a) shows the first soliton, the second soliton, and the formation of the third soltion. (b) is the magnification of the third soliton. The solutions computed by the proposed method is compared with those computed by the particle method. The results are indistinguishable between the two methods.

### 5.4.2 Soliton-antisoliton collision

The two-soliton dynamics of the non-dispersive CH equation (5.11) are studied in detail in [2,3]. An exact solution is given for the perfectly antisymmetric "soliton-antisoliton" collision case. This is a numerically challenging problem, since the term $uu_{xx}$ tends toward a sum of delta functions when the collision occurs. This suggests that the right-hand-side of equation (1.3) becomes the derivative of a delta function when the collision occurs. Similar to the previous example, we avoid the numerical difficulty by using the α-formulation in our numerical simulations.

Consider the soliton-antisoliton initial condition

$$u_0(x) = e^{-|x+5|} - e^{-|x-5|}. \tag{5.15}$$

The collision time $t_c$ and the wave speed $c$ can be obtained by solving equation (4.26) in [3]

$$\begin{aligned} 10 &= -2\log\left[\operatorname{sech}(-ct_c)\right], \\ 2 &= \frac{-2c}{\tanh(-ct_c)}. \end{aligned} \tag{5.16}$$

Solving the above equations, we have $c \simeq 0.999977299777468$ and $t_c \simeq 5.693265068768256$. Following the notations in [3], we write the solution of equation (5.11) for the soliton-antisoliton collision as

$$u(x,t) = \frac{c}{\tanh\left(c(t-t_c)\right)}\left[e^{-|x-q(t)|} - e^{-|x+q(t)|}\right], \tag{5.17}$$

where

$$q(t) = -\log\left[\operatorname{sech}^2(t-t_c)\right]. \tag{5.18}$$

Figure 5.5 (a) − (d) show simulations of the soliton-antisoliton collision: (a) is the initial condition, (b) is the beginning of the collision, (c) is the approximate time of the collision, and (d) is post collision. The

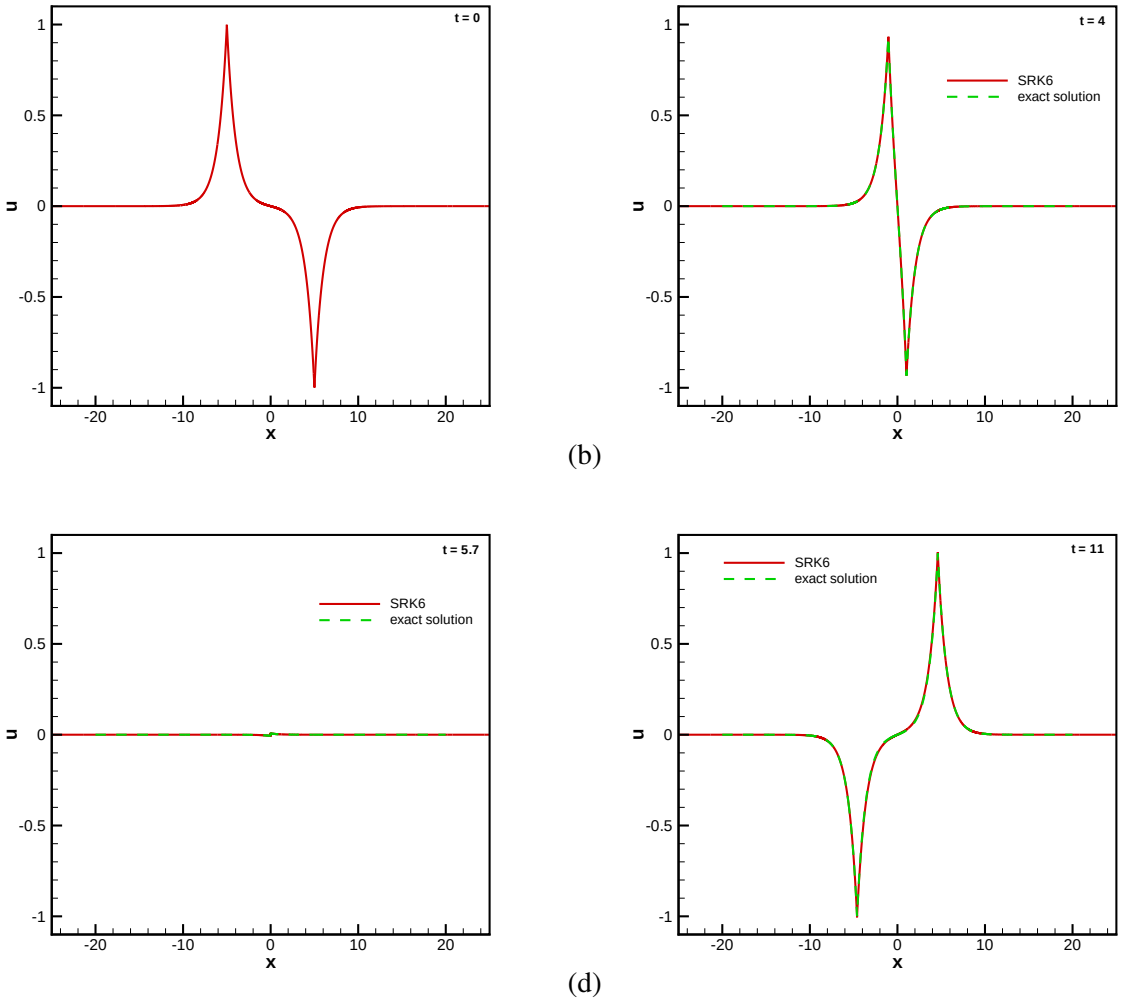


Figure 5.5: The soliton-antisoltoin collision: (a) is the initial condition, (b) is the beginning of the collision, (c) is the approximate time of the collision, and (d) is post collision. The theoretical wave speed is $c \simeq 0.999977$, and the theoretical collision time is $t_c \simeq 5.69327$. The computed solutions are compared with the exact solutions in the Figures. The simulation figures show that the proposed scheme not only accurately captures the wave speed and the collision time, but they are indistinguishable from the exact solutions.

Figures compare solutions computed by the proposed scheme with the exact solutions found by equations (5.17) and (5.18). They show that the proposed scheme not only accurately captures the wave speed and the collision time, but they are indistinguishable from the exact solutions. The number of cells used in the simulations is $N = 16384$ in the domain $[-25, 25]$, or $\Delta x \cong 0.003051$. The time step is $\Delta t = 0.001$.

# 6 Conclusion and future work

A two-step iterative algorithm for a completely integrable CH equation is developed in this study. The algorithm is sixth-order accurate and preserves the dispersion relation and the Hamiltonians of the equation. In the first step, we introduce a sixth-order accurate dispersion-relation-preserving scheme to approximate the first-order spatial derivatives, and in the second step we develop a three-point sixth-order accurate Helmholtz solver. A sixth-order symplectic Runge-Kutta time integrator that well preserves the Hamiltonians of the completely integrable CH equation is employed as the time-stepping scheme in the first step. Strength of the proposed algorithm is validated through several examples to demonstrate the method's efficiency and accuracy over time. We assess the computational quality of the proposed algorithm by the computed errors, the CPU times, and the rates of convergence. Note that for peakon or peakon-like solutions, such as the examples in Sections 5.4.1 and 5.4.2, it makes sense to implement some type of adaptive-mesh-refinement (AMR) scheme to resolve the sharp peaks, in particular for the Eulerian type of schemes like the proposed algorithm. However, since this study is a one-dimensional problem, instead of an AMR scheme, we use very fine grids to resolve the peakon type of solutions, while maintaining reasonable computational times.

While we have developed an efficient higher-order method to study solution properties of the CH equation, there are still questions left unanswered by this study. One of them regards the splitting errors introduced by the two-step iterative process. The two-step iterative method developed here is similar to operator splitting methods. It is not clear what splitting error is introduced by solving two equations alternately. We are developing a posterior error estimator to evaluate the splitting error introduced by the iterative scheme.

# 7 Acknowledgment

This work was supported by the National Science Council of the Republic of China under Grants NSC96-2221-E-002-004 and partially supported by NSF through the Grant DMS-0610149. T. W. H. Sheu would like to thank the Department of Mathematics at the University of Wyoming in Laramie for its provision of excellent research facilities during his visiting professorship. In addition, we were stimulated considerably by the discussion with R. Camassa in the course of conducting this study.

# References

[1] R. Artebrant and H. J. Schroll, Numerical simulation of Camassa-Holm peakons by adaptive upwinding, Appl. Numer. Math., 56 (2006) 695-711.

[2] R. Camassa and D. Holm, An integrable shallow water equation with peaked solitons, Phys. Rev. Letters, 71 (1993) 1661-1664.

[3] R. Camassa, D. Holm, and J. M. Hyman, A new integrable shallow water equation, Advan. Appl. Mech., 31 (1994) 1-33.

[4] R. Camassa and A.I. Zenchuck, On the initial value problem for a completely integrable shallow water wave equation, *Phys. Lett. A*, 281:26–33, 2001.

[5] R. Camassa, Characteristics and initial value problem of a completely integrable shallow water equation, DCDS-B, 3 (2003) 115-139.

[6] R. Camassa, J. Huang, and L. Lee, On a completely integral numerical scheme for a nonlinear shallow-water wave equation, J. Nonlin. Math. Phys., 12 (2005) 146-162.

[7] R. Camassa, J. Huang, and L. Lee, Integral and integrable algorithm for a nonlinear shallow-water wave equation, J. Comp. Phys., 216 (2006) 547-572.

[8] R. Camassa and L. Lee, A complete integral particle method for a nonlinear shallow-water wave equation in periodic domains, DCDIS-A, 14(S2) (2007) 1-5.

[9] R. Camassa and L. Lee, Complete integrable particle methods and the recurrence of initial states for a nonlinear shallow-water wave equation, J. Comp. Phys., 227 (2008) 7206-7221.

[10] R. Camassa, P. H. Chiu, L. Lee, and T. W. H. Sheu, Numerical investigation of Helmholtz regularizations in a class of partial differential equations, in submission.

[11] P. H. Chiu, L. Lee, and T. W. H. Sheu, A dispersion-relation-preserving algorithm for a nonlinear shallow-water wave equation, *J. Comput. Phys.* 228 (2009) 8034-8052.

[12] G. M. Coclite, K. H. Karlsen and N. H. Risebro, A convergent finite difference scheme for the Camassa-Holm equation with general $H^1$ initial data, Dept. Math. /CMA University of Oslo, 16 (2006) 1-34.

[13] D. Cohen, B. Owren, and X. Raynaud, Multi-symplectic integration of the Camassa-Holm equation, J. Comp. Phys., 227 (2008) 5492-5512.

[14] J. De Frutos and J. M. Sanz-Serna, An easily implementable fourth-order method for the time integration of wave problems, J. Comput. Phys., 103 (1992) 160-168.

[15] H. Holden and X. Raynaud, A convergent numerical scheme for the Camassa-Holm equation based on multipeakons, DCDS-B, 14 (2006) 503-523.

[16] H. Holden and X. Raynaud, Convergence of a finite difference scheme for the Camassa-Holm equation, SIAM J. Numer. Anal., 44 (2006) 1655-1680.

[17] R.S. Johnson Camassa-Holm, Korteweg-de Vries and related models for water waves, JFM, 455 (2002) 63-82.

[18] H. Kalisch and J. Lenells, Numerical study of traveling-wave solutions for the Camassa-Holm equation, Chaos, Solitons & Fractals, 25 (2005) 287-298.

[19] H. Kalisch and X. Raynaud, Convergence of a spectral projection of the Camassa-Holm equation, Numerical Methods for Partial Differential Equations, 22 (2006) 1197-1215.

[20] J. Lenells, Conservation laws of the Camassa-Holm equation, J. Phys. A., 38 (2005) 869-880.

[21] W. Oevel, W. Sofroniou, Symplectic Runge-Kutta schemes II: classification of symplectic methods, *Univ. of Paderborn, Germany, Preprint*, 1997.

[22] C. K. W. Tam and J. C. Webb, Dispersion-relation-preserving finite difference schemes for computational acoustics, J. Comp. Phys., 107 (1992) 262-281.

[23] Y. Xu and C. W. Shu, A local discontinuous Galerkin method for the Camassa-Holm equation, SIAM J. Numer. Anal., 46 (2008) 1998-2021.

[24] N. J. Zabusky and M. D. Kruskal, Interaction of "solitons" in a collisionless plasma and the recurrence of initial states, *Phys. Rev. Lett.*, 15 (1965) 240-243.